Journal of Materials Chemistry C

Accepted Manuscript

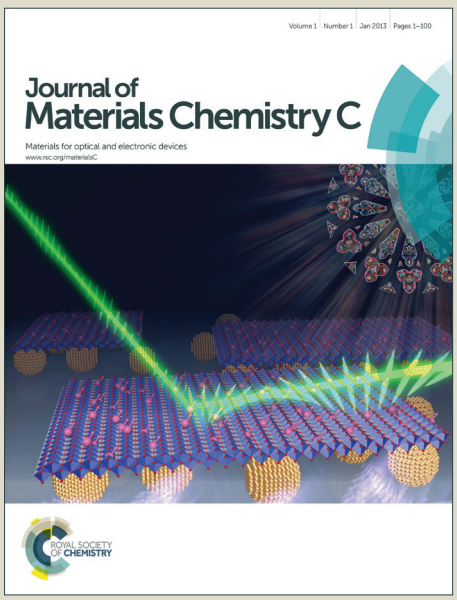

ROYAL SOCIETY OF CHEMISTRY

www.rsc.org/materialsC

Cite this: DOI: 10.1039/c0xx00000x

ARTICLE

www.rsc.org/xxxxxx

Nanostructured $La_{0.7}Sr_{0.3}MnO_3$ compound for effective Electromagnetic Interference shielding in X-band frequency range

Hilal Ahmad Reshi[1], Avanish P Singh[2], Shreeja Pillai[1], Rama Shankar Yadav[1], S. K. Dhawan[2] and Vilas Shelke[1,3]*

[1] *Novel Materials Research Laboratory, Department of Physics, Barkatullah University, Bhopal 462026 (M.P.) INDIA*
[2] *Polymeric and Soft Materials Section, CSIR-National Physical Laboratory, Dr. K S Krishnan Road, New Delhi 440012, INDIA*
[3] *Department of Materials Science and Nanoengineering, Rice University, Houston 77005 TX, USA*
**drshelke@gmail.com*

Received (in XXX, XXX) Xth XXXXXXXXX 20XX, Accepted Xth XXXXXXXXX 20XX
DOI: 10.1039/b000000x

We report detailed study on the electromagnetic interference (EMI) shielding effectiveness (SE) properties in $La_{0.7}Sr_{0.3}MnO_3$ (LSMO) nanomaterials. The samples were prepared by solution chemistry (Sol-Gel) route with different sintering temperatures. The single-phase samples with grain size 22 and 34 nm showed dc electrical conductivity variation from 0.65 to 13 S/cm at room temperature. An application of high magnetic field resulted in higher conductivity values. The electrical conductivity variation with temperature could be fitted with variable range hopping mechanism in limited range of temperature. The variation of frequency dependent electromagnetic parameters measured at room temperature within the X-band region is consistent with electrical conductivity behavior. The complex permittivity and permeability parameters were determined in line with Nicholson-Ross and Weir algorithms. The LSMO nanomaterial samples showed EMI shielding effectiveness value up to 19 dB (96.3 % attenuation) over X-band frequency range suitable for microwave radiation shielding in commercial and defense appliances.

Introduction

The inevitable use of several personal electronic gadgets, home appliances, commercial/industry equipments have created electromagnetic radiation pollution. The adverse effect of Electromagnetic Interference (EMI) on the electronic functionality and human health has triggered search for suitable absorbing materials. The rapid development of wireless telecommunication, local area networks, radar navigation and many home appliances necessitate improvement of electromagnetic interference shielding. The EM wave absorbing materials are required to have a strong absorption over a wide range of frequency and should be lightweight, flexible, corrosion resistant, cost effective and easy to process. A variety of nanomaterials including carbon nanotubes, graphene oxides, transition metal oxides and their composites have been studied in the recent years for this purpose[1-10]. There are number of aspects like conducting, grounding, electrostatic discharge (ESD), etc which contribute to the overall performance of the shielding materials. An extensive amount of studies have been devoted to explore highly efficient materials that attain a good quality of EMI radiation absorption properties. To provide an adequate solution for EMI problem, it is observed that the materials with moderate electrical conductivity and dielectric nature can contribute to high EMI shielding effectiveness (SE)[11-13]. A material with incipient electric and magnetic dipole moments may also be suitable candidate for electromagnetic radiation absorption.

Ferromagnetic materials are important for modern technological applications in all kinds of domestic power to high speed electronic devices[14]. Magnetic materials possess tuneable conductivity and magnetism making them promising candidates for microwave absorption materials. In particular, doped perovskite manganites have attracted wide attention due to their unique properties, such as colossal-magnetoresistance (CMR), metal-insulator transition, and spin-polarized conduction. We have studied several physical properties of these materials in bulk form[15-18]. A rare-earth manganite with composition $La_{0.7}Sr_{0.3}MnO_3$ (LSMO) is a fascinating material as it possesses a unique combination of electrical and magnetic properties. Such compounds also show distinct features when synthesized in nanomaterial form[19,20]. The tendency of these materials to localize or delocalize charge carriers; order and reorder magnetic moments with external stimuli like temperature, magnetic field, etc motivated us to study them for electromagnetic radiation shielding. An epoxy composite of bulk LSMO has been reported

to show microwave shielding with peak reflection loss of 23 dB at 10.5 GHz[21]. The negative permittivity, one of the interesting features has been observed in LSMO with variable Sr content[22]. Similarly, Zang and Cao reported microwave absorption in transition metal doped LSMO compound[23]. In these studies, the shielding efficiency was high around narrow frequency band. However, a material will be more suitable for device applications, if the response is consistent over wide range of frequency. In this paper, we report synthesis of LSMO nanoparticles through chemical route. The crystal structure, morphologies, electrical conductivity, electromagnetic scattering parameters and EMI shielding effectiveness were examined. The pristine samples without any substitution or composite formation showed EMI shielding efficiency (SE) around 19 dB (96.3 % attenuation) over wide microwave frequency range (X-band).

Experimental Procedure

LSMO nano-powder with nominal composition $La_{0.7}Sr_{0.3}MnO_3$ was prepared by well known sol-gel route. Stoichiometric amounts of Lanthanum (II) acetate hydrate (99.9%), strontium acetate (99.5%) and manganese (II) acetate tetra hydrate (99%) were dissolved in distilled water with acetic acid and ethylene glycol to obtain individual transparent solution precursors. These precursors were mixed drop wise at room temperature through continuous stirring. Ammonium acetate was added to enhance the homogeneity and maintain the pH around neutral range. This mixture was heated slowly at 80 °C to evaporate the excess water and to obtain a gel. A brown-black coloured powder was formed after heating the gel at 110 °C. The powder was ground manually for two hours and calcinated at 500 °C for 12 hours. The calcinated mass was pressed into 12mm diameter pellets. The pellets were divided into two batches sintered at 600 °C (LSM6) and 800 °C (LSM8) in air ambient for 2 hours.

We used X-ray diffractometer (D8 advanced Bruker) with CuK_α radiation (λ=1.54 Å) to determine phase purity and crystal structure of samples. The X-ray diffraction patterns were analyzed by Rietveld refinement using FULLPROF package. The dc electrical conductivity measurements were done by four probe method using commercial cryostat (Oxford Instruments Inc., UK) in the temperature range 10K to 300K with and without high magnetic field. The nanostructure of the LSMO particles was observed using Transmission Electron Microscopy (TEM). An Agilent E8362B vector network analyzer was used to explore the EMI shielding compatibility of the LSMO nanoparticles in X-band frequency range. The powder samples were palletized in a rectangular die with dimensions 22 x10 mm^2 of thickness ~2mm and loaded into a copper sample holder connected between the wave-guide flanges of network analyzer.

Results and discussion

Structural

The X-ray Diffraction (XRD) patterns revealed the formation of single phase compound for the samples sintered at 600 (LSM6) and 800 (LSM8) ^{0}C as shown in Fig. 1 a). A representative Rietveld refined graph of LSM6 sample is shown in Fig. 1 b). The Rietveld refinement confirmed orthorhombic perovskite structure with a space group *Pnma*. The structural parameters for both samples are given in Table 1. Since chemical composition and calcinations temperature were the same for both samples, they did not show any significant change in lattice parameters. A goodness of fit values below 2 illustrated a good agreement between the observed and calculated data. It also pointed out that LSMO can be synthesized by sol-gel method even at relatively low temperature 600 °C. According to the phase diagram of bulk rare earth manganite the $La_{0.7}Sr_{0.3}MnO_3$ composition should show a rhombohedrally distorted (R3C) perovskite structure. However, nanomaterials sample with the same composition shows orthorhombic structure[19].

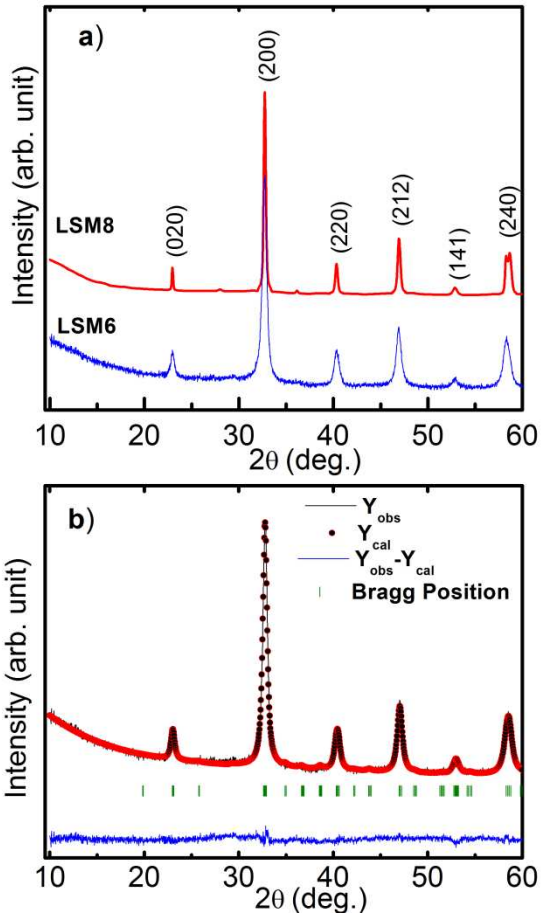

Fig.1 X-Ray Diffraction patterns of a) LSM6 and LSM8 samples and b) representative Rietveld refined XRD pattern.

Table 1 refined structural parameters obtained from Rietveld refinement analysis.

Parameters		LSM8	LSM6
a (Å)		5.342	5.446
b (Å)		7.711	7.712
c (Å)		5.601	5.487
V (Å^3)		230.717	230.518
La^{+3}	x	0.0109	0.0148
	y	0.2500	0.2500
	z	0.0070	0.0114
Mn^{+3}	x	0.0000	0.0000
	y	0.0000	0.0000
	z	0.5000	0.5000
O_1^{-2}	x	0.4108	0.5041
	y	0.2500	0.2500
	z	-0.0731	-0.0090
O_2^{-2}	x	0.3801	0.2009
	y	-0.0192	0.0221
	z	-0.3365	0.6819
R_{wp}		6.13	4.16
R_p		5.09	5.36
R_e		13.91	13.83
R_{Bragg}		5.68	7.91
χ^2		1.57	1.54

Microstructure

The grain morphology is very important to facilitate electromagnetic absorption properties because grain boundaries act as electromagnetic wave attenuation centres leading to electric/magnetic loss[24]. Figure 2 a) and b) are the TEM images of LSM6 and LSM8 samples along with their Selected Area Electron Diffraction (SAED) patterns respectively. The grain size distribution is quite narrow with distinctly dispersed nanoparticles. The average grain sizes for LSM6 and LSM8 were 22 and 34 nm respectively. The variation in grain size from 22 to 34 nm with higher sintering temperature is relevant to the increased grain growth.

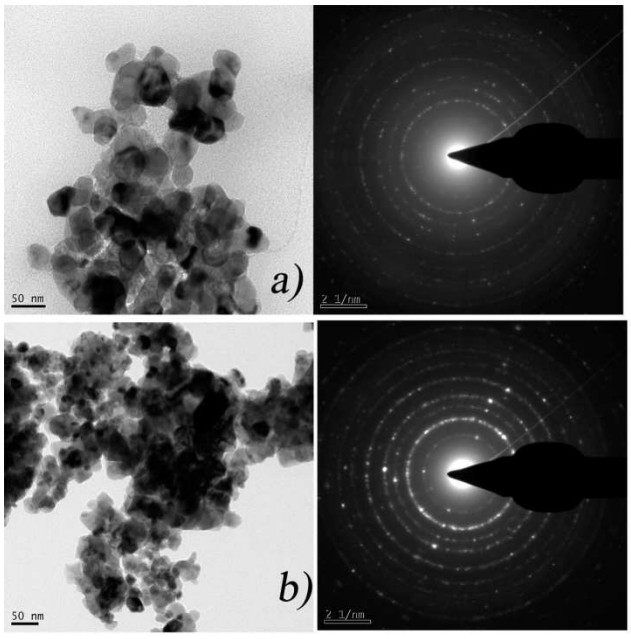

Fig.2 Transmission Electron microscopy images of a) LSM6 and b) LSM8 sample with SAED patterns

Electrical Conductivity

The figures 3 a) and b) indicate temperature dependent variation of dc electrical conductivity (σ) for LSM8 and LSM6 samples respectively. For sample LSM8, the conductivity values decrease with temperature in the range 300-200 K and then increase up to 50 K before showing further decline. The transition from semi-conductor to metallic behaviour around 200 K is slightly unusual as bulk LSMO is not known to show metal-insulator (or semiconductor) transition[15]. The finite size effect and excessive scattering of charge carriers from grain boundaries should be responsible for such behaviour. The sample LSM6 with lower grain size showed lower conductivity values and mostly reduction in conductivity with temperature. The zero-field conductivity value for LSM8 (13.8 S/cm) is around twenty times higher than that of LSM6 (0.63 S/cm) at room temperature. The effect of magnetic field on conductivity behaviour in these samples is noteworthy. In both samples, conductivity values increase profoundly with applied magnetic field over entire range of temperature. In spite of large difference in zero-field conductivity, both samples retained the typical characteristic of magneto-conductivity in LSMO system. Positive magneto-conductivity (negative magnetoresistance) is observed at different magnetic fields.

According to percolation theory, the electrical conductivity is determined by the ability of a material to form a conducting path. In LSM8 larger grain size reduces the population of grain interfaces, which act as scattering centres, leading to high conduction network. The difference between the conductivities makes significant variation in radiation shielding effectiveness of the material. The improvement of electrical conductivity plays a vital role for effective electromagnetic shielding[25]. The results suggest that moderate conductivity enhances EMI shielding efficiency (SE). It has been observed that introduction of conducting powders through chemical doping or mixing increases the EMI SE[26]. It is important to understand the conductivity mechanism of our samples, in the range near room temperature. The response of our samples has been analyzed by variable range hopping (VRH) transport mechanism[27]. The temperature dependent conductivity can be expressed as

$$\sigma = \sigma_0 \exp\left[(-T_0/T)^{1/4}\right] \quad (1)$$

where T_0 is the measure of the Mott characteristic temperature representing the hopping barrier and σ_0 is conductivity at infinite temperature. The Figures 3 c) and d) shows the plots of (ln σ) versus $T^{-1/4}$ for LSM8 and LSM6 samples in semiconducting region near room temperature. Both samples showed linear fit which, indicated that VRH is an appropriate transport mechanism in this region. The relevant fitting parameters are mentioned in table 2. Around room temperature, the conductivity is governed by the hopping of charge carriers. The effective amplitude of hopping is different in the two samples. The conceptual hypothesis of metallic droplets in dielectric matrix can explain the size quantization effect up to some extent[27]. The smaller grain sample has higher inter-granular tunnelling and electrostatic barriers than the larger grain sample. Consequently, it is expected to show lower conductivity.

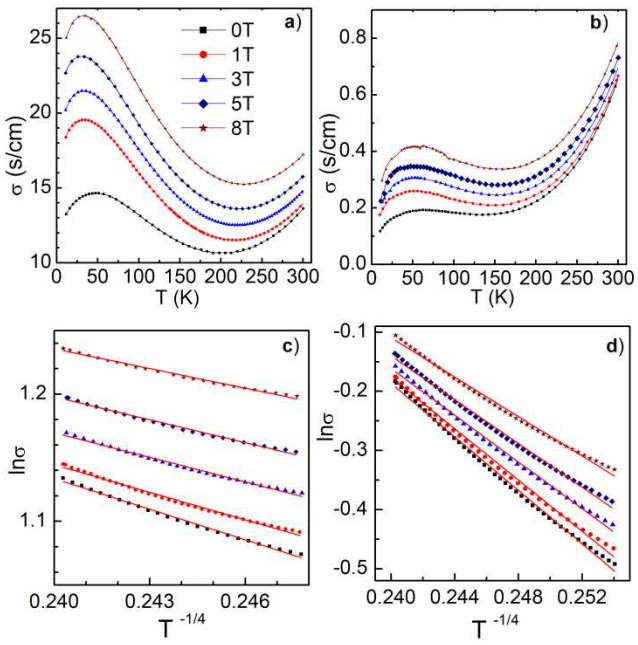

Fig.3 Variation of dc conductivity (σ) as a function of temperature- a) σ verses T of LSM8 sample, b) σ verses T of LSM6 sample, c) (ln σ) verses $T^{-1/4}$ of LSM8 and d) (ln σ) verses $T^{-1/4}$ of LSM6

Table 2. Magnetic field (H) dependant DC conductivity (σ) at 300 K and 10 K along with VRH parameters for LSMO samples.

Sample	H (tesla)	σ at 300 K (S/cm)	σ at 10 K (S/cm)	σ_0 (S/cm)	T_0 (K)
LSM8	0	13.80	13.24	3.05	4.11×10^3
	1	14.00	18.40	2.87	2.70×10^3
	3	14.76	20.15	2.71	1.69×10^3
	5	15.70	22.65	2.63	1.28×10^3
	8	17.22	25.01	2.47	0.70×10^3
LSM6	0	0.63	0.11	5.23	25.94×10^4
	1	0.67	0.17	5.02	22.05×10^4
	3	0.69	0.20	4.57	15.15×10^4
	5	0.73	0.22	4.29	11.63×10^4
	8	0.77	0.29	3.88	7.70×10^4

Complex Parameters

The frequency dependent variations of electromagnetic parameters viz., complex permittivity ($\varepsilon^* = \varepsilon' - i\varepsilon''$) and complex permeability ($\mu^* = \mu' - i\mu''$) are shown in figure 4. More details of such conversion and analysis are available in literature[28, 29]. The measurements were carried out on homogeneous powder sample with density around 3.4 gm/cm^3. Apparently, no filler-matrix type of composite was used. It is seen from figure 4 a)-b) that real (ε') and imaginary (ε'') permittivity values are higher for LSM8 sample as compared to LSM6. Fig. 4 c) and d) show the variation in real (μ') and imaginary (μ'') parts of complex permeability respectively. The real permeability (μ') shows decreasing trend with intermittent peaks/dips as frequency increases. The permittivity and permeability parameters were used to determine the dielectric and magnetic tangent loss of samples are shown in figure 4 e) and f) respectively. The dielectric tangent loss ($\tan\delta_e$) is higher in LSM8 than LSM6 sample. The magnetic tangent loss ($\tan\delta_m$) is higher in LSM8 than LSM6 sample at lower frequency.

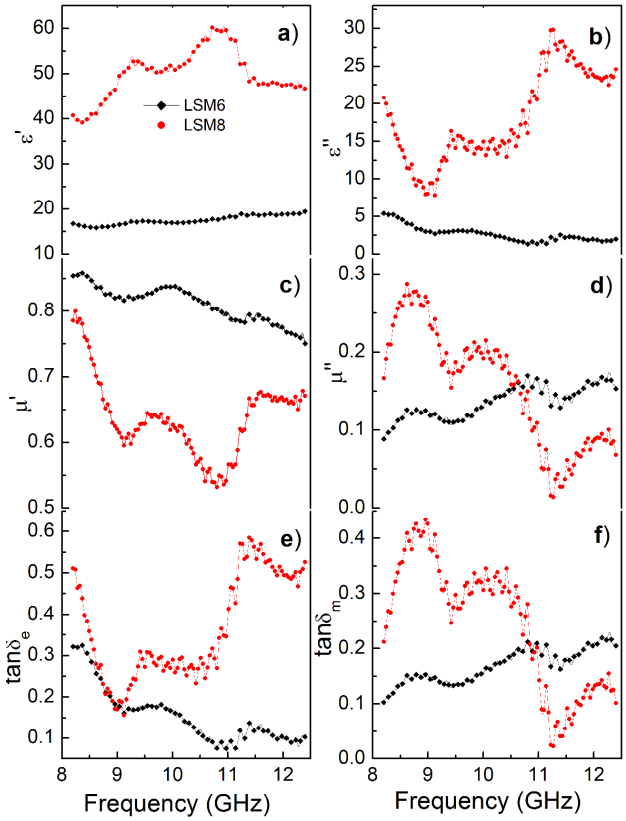

Fig. 4 Frequency dependent a) real and b) imaginary parts of complex permittivity; c) real and d) imaginary parts of complex permeability; corresponding e) dielectric and f) magnetic loss tangents of LSMO samples.

The real EM parameters (ε' and μ') are directly associated with the storage ability of electric and magnetic energy while the imaginary ones (ε'' and μ'') represent the dissipation of electric and magnetic energy respectively. The permittivity generates from electronic, ionic, space-charge, and interfacial polarization, which means that permittivity, is a measure of polarizability of a material[30, 31]. The increase in permittivity can be attributed to the increase in carrier concentration and conductivity[32]. The complex fluctuation observed in permittivity of LSM8 sample over the measured frequency range suggests a resonance behavior expected in conductive materials as a consequence of skin effect[33,34]. This behavior could also be related to electron hopping between Mn^{+3}-O-Mn^{+4} ions at the applied EM wave frequency[35,36]. In comparison with other materials[37-41], both real and imaginary parts of LSM6 and LSM8 samples are high, indicating dielectric storage and loss of electromagnetic wave. The increase of both real and imaginary parts of dielectric permittivity contributes towards enhancement of total shielding efficiency. The dielectric loss mechanism includes complex phenomena like natural resonance loss, dielectric relaxation loss, conduction loss, electronic polarization and its relaxation etc.[42-44]. Moreover, the dielectric loss is improved by polaron hopping and bound charges which restrict the mobility and account for strong polarization in the material[45,46]. Similarly, the wavy nature of permeability is indicative of magnetic resonance. The appearance of clear peaks in imaginary permeability (μ'') also implies stronger resonance in LSM8 than LSM6 sample [47]. Increase in μ''

of LSM6 sample with frequency is caused by the time lag of magnetization vector behind the magnetic field vector. The change in magnetization vector is generally brought by the rotation of magnetization. These motions lag behind the change in the magnetic field and contribute to the magnetic loss[45]. The enhancement of number of atoms with dangling bonds and surface area leads to the interface polarization due to accumulation of charges at the interface. It plays significant role for the microwave absorption[47,48]. The observed dielectric tangent loss is above 0.1 throughout the measured frequency range, revealing that dielectric loss occurs over wide range. The magnetic tangent loss (tan δ_m) rises gradually in whole frequency range for LSM6 where as it fluctuates for LSM8 and shows better value than LSM6 below 10.6 GHz. It illustrates that LSM8 sample exhibits more dielectric loss at higher frequency and more magnetic loss at lower frequency as compared to LSM6 sample.

EMI shielding effectiveness

The EMI shielding effectiveness (SE) of a material is expressed in terms of ratio of incident and transmitted energy and can be represented mathematically in logarithmic scale given by

$$SE_T\ (dB) = -10\log\{P_T/P_I\} = -10\log\{E_T/E_I\} = -10\log\{H_T/H_I\} \quad (2)$$

where P_I (E_I or H_I) and P_T (E_T or H_T) are the power (electric or magnetic field) of incident and transmitted electromagnetic waves respectively. The total shielding effectiveness SE_T is a contribution of three components viz Absorption (SE_A), Reflection (SE_R) and multiple internal reflection (SE_M). The reflection (R) transmission (T) and Absorption (A) components were obtained through the measurement of scattering parameters S11 (or S22) and S21 (or S12) of a two port network analyzer, where $R = |S11|^2$ and $T = |S21|^2$ and $A = 1 - |S11|^2 - |S21|^2$. The total shielding effectiveness, SE_T of samples is given by

$SE_T = SE_R + SE_A + SE_M$

$$SE_R = -10\log(1-R),\ SE_A = -10\log(T/1-R)$$

and $$SE_M = -20\log(1-10^{-SEA/10}) \quad (3)$$

The multiple reflection term (SE_M) can be ignored in case $SE_T >$ 10 dB or if the shield is thicker than the skin depth[49,50]. The multiple reflections term is considered for large surface areas as in porous or foam materials and is not significant in the present study. The primary mechanism for EMI shielding is reflection for which the shield possesses mobile charge carriers that can interact with electromagnetic waves. The shield needs electrically moderate conductivity around 10^{-3} to 1 S/m[51, 52]. The strong and effective secondary mechanism is absorption resulting from interaction of electric/magnetic dipoles with electromagnetic radiations. Figure 5 shows the frequency dependence of EMI shielding effectiveness along with total attenuation values for both samples. The experimental measurements reveal that shielding effectiveness due to absorption (SE_A) and reflection (SE_R) varies from 12.3dB to 14.1dB and 6dB to 4.3dB in LSM8, whereas from 5.5dB to 7 dB and 6.5dB to 2.2dB in LSM6 respectively. The maximum values of total shielding effectiveness (SE_T) achieved for the LSM8 and LSM6 samples are 19dB and 13dB, which corresponds to an attenuation of 96.3 % and 77.4 % respectively. In both samples, SE_R decreases and SE_A increases with the increase in frequency. Therefore, the total shielding effectiveness remains almost constant in the entire frequency range. A uniform shielding over a wide range of frequency is the prominent feature of these samples. By increasing sintering temperature, conductivity also increases and SE_T increases from 12.9 to 19 dB as shown in figure 5. These results, associated with the dielectric and magnetic parameters in figure 4, indicate that improvement of magnetic and dielectric properties of LSMO nanostructures has significant effect on the improvement of microwave range shielding efficiency.

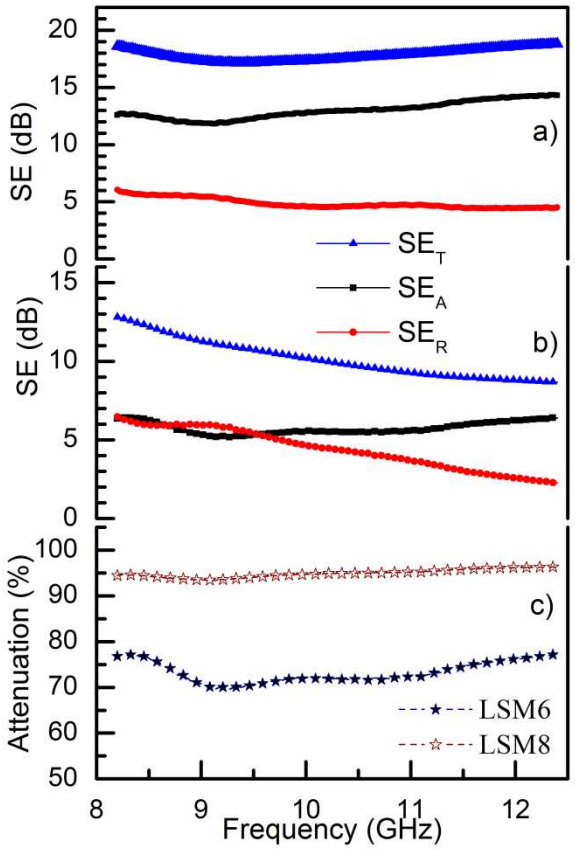

Fig.5 Frequency dependent electromagnetic shielding effectiveness of a) LSM8, b) LSM6 and c) attenuation value for both the compounds.

The theoretical understanding of intricate mechanism of EMI shielding is beyond the scope of present study. A detailed analysis based on forward/backward propagation matrices inserted with generic algorithm and effective theoretical design for nanoparticle filler have been reported by Micheli et al.[53,54] Qualitatively, the real part of permittivity is strongly related to electric charge accumulation due to interfacial polarization effects and imaginary part is due to loss effects[55]. The conduction or quantum mechanical tunnelling currents contribute for the losses. At high frequency (f), electromagnetic radiation penetrates only at the near surface region of the sample. The electric field of a plane wave drops exponentially with increasing depth in to the material. The depth at which the field drops to 1/e of the incident value is called the skin depth (δ). The ac conductivity (σ_{ac}) and skin depth (δ) are related to imaginary permittivity (ε'') and real permeability (μ') as $\sigma_{ac} = 2\pi f\varepsilon_0\varepsilon''$ and $\delta = (2/\sigma_{ac}2\pi f\mu')^{1/2}$. In order to find out the effect of conductivity on shielding parameters, we plotted σ_{ac} against the measured frequency range (fig. 6 a).

Usually, the shielding effectiveness can be enhanced by increasing metal layer or the conductivity[56]. The conductivity shows oscillatory behaviour for both the samples and is higher for LSM8 than LSM6 sample. The variation of skin depth δ with frequency is shown in figure 6 b). The skin depth increases with frequency initially for both samples, which demonstrates a lack of surface conduction. However, in LSM8, the skin depth decreases with increase in frequency, which reveals that surface conduction may improve at higher frequencies. Conductivity and magnetic permeability of the material plays a significant role in reducing or enhancing the skin depth. The maximum skin depth of LSM6 is around 6 mm while that of LSM8 is 3.4 mm. The samples showing optimum value of conductivity and magnetization is desirable for exhibiting good microwave shielding applications[57].

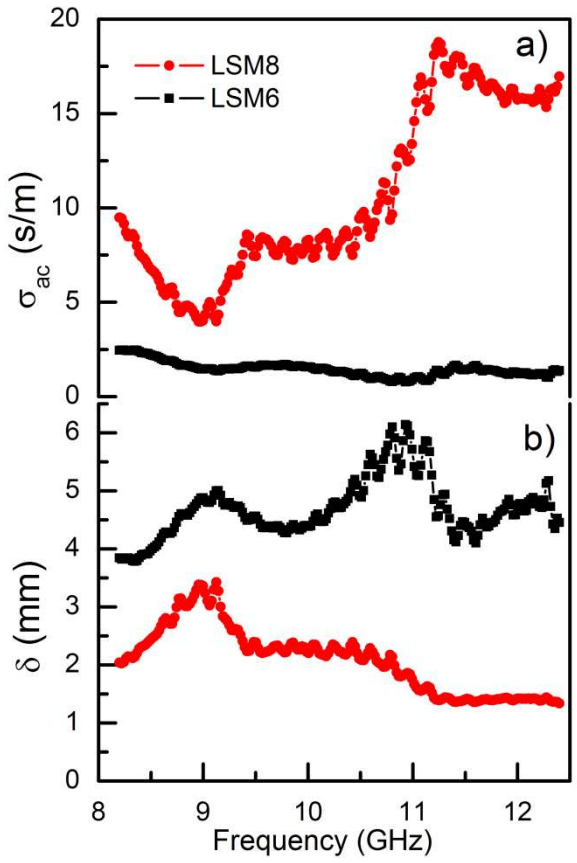

Fig.6 The frequency dependent variation of a) ac conductivity (σ_{ac}) and b) skin depth (δ) for LSM8 and LSM6 samples.

Conclusions

We synthesized LSMO nanoparticles by solution chemistry (Sol-Gel) route with grain sizes 22 and 34 nm. The nanomaterial samples showed phase pure compound with orthorhombic Pnma crystal structure. The samples showed metal-insulator transition and magneto-conductivity effects. The semiconducting region follows variable range hoping transport mechanism. The variation of permittivity suggests a resonance behavior observed in conducting materials while permeability manifests the magnetic energy storage and loss. The total shielding effectiveness values of 19 (96.3 % attenuation) and 13 dB (77.4 % attenuation) have been achieved in two samples over X-band frequency range. The high value of shielding effectiveness is mostly dominated by absorption rather than reflection. The occurrence of significant shielding effectiveness illustrated that nano LSMO is promising oxide materials for EMI shielding in microwave frequency range.

Acknowledgement

This work is financially supported by M. P. Council of Science and Technology, Bhopal and the University Grants Commission, New Delhi. A part of the work was performed at UGC-DAE Consortium for Scientific Research, Indore, India. The authors are thankful to Dr. Mukul Gupta and Dr. Rajiv Rawat for providing experimental facilities.

Notes and References

1. B. Shen, W. Zhai, and W. Zheng, *Adv. Funct. Mater.* 2014, DOI: 10.1002/adfm.201400079
2. N. Yousefi, X. Sun, X. Lin, X. Shen, J. Jia, B. Zhang, B. Tang, M. Chan, and J.K. Kim, *Adv. Mater.* 2014, DOI: 10.1002/adma.201305293
3. B. Wen, M. Cao, M. Lu, W. Cao, H. Shi, J. Liu, X. Wang, H. Jin, X. Fang, W. Wang, and Jie Yuan, *Adv. Mater.* 2014, DOI: 10.1002/adma.201400108
4. N. Li, Y. Huang, F. Du, X. He, X. Lin, H. Gao, Y. Ma, F. Li, Y. Chen, and C. Eklund, *Nano Lett.*, 2006, **6**, 1141.
5. J. Zhu, S. Wei, L. Zhang, Y. Mao, J. Ryu, N. Haldolaarachchiqe, D. P. Young, and Z. Guo, *J. Mater. Chem.*, 2011, **21**, 3952
6. X. Li, L. Zhang and X. Yin, *J. Am. Ceram. Soc.*, 2012, **95**, 1038.
7. A. P. Singh, M. Mishra, A. Chandra, and S. K. Dhawan, *Nanotechnology*, 2011, **22**, 465701.
8. A. P. Singh, M. Mishra, P. Sambyal, B. K. Gupta, B. P. Singh, A. Chandra, and S. K. Dhawan, *J. Mater. Chem. A*, 2014, **2** 3581.
9. Y. J. Chen, G. Xiao, T. S. Wang, Q. Y. Ouyang, L. H. Qi, Y. Ma, P. Gao, C. L. Zhu, M. S. Cao, and H. B. Jin, *J. Phys. Chem. C*, 2011, **115,** 13603.
10. G. Tong, W. Wu, Q. Hua, Y. Miao, J. Guan, and H. Qian, *J. Alloy. Compd.*, 2011, **509,** 451.
11. Manuela Loeblein , Roland Yingjie Tay , Siu Hon Tsang , Wei Beng Ng, and Edwin Hang Tong Teo, *small* 2014, DOI: 10.1002/smll.201400292
12. H. M. Kim, K. Kim, C. Y. Lee, J. Joo, S. J. Cho, H. S. Yoon, D.A. Pejakovic, J. W. Yoo, and A. J. Epstein, *Appl. Phys. Lett.*, 2004, **84**, 589.
13. R. Che, L. M. Peng, X. Duan, Q. Chen, and X. Liang, *Adv. Mater.*, 2004, **16**, 401.
14. N. A. Spaldin, "Magnetic materials: Fundamentals and applications," Cambridge University press, New York, (2011) p 270
15. V. Shelke, A. Das, I. Dhiman, R. Yadav, S. Khatarkar, A. Anshul, and R. K. Singh, *J. Phys.: Conden. Matter.*, 2008, **20**, 395218.
16. V. Shelke, S. Khatarkar, R. Yadav, A. Anshul, and R. K. Singh, *J. Magn. Magn. Mater.*, 2010, **322**, 1224.
17. R. Yadav, A. Anshul and V. Shelke. *J. Mater. Sci. Mater Electron*, **22**, 1173, (2011)
18. Reena Singh, D. Bhuwal, R. Yadav, S. Khatarkar, Vilas Shelke, *IEEE Trans. Magn.*, 2012, **48**, 1155.
19. H. A. Reshi, S. Pillai, D. Bhuwal, and V. Shelke, *J. Nanosci. Nanotechnol.*, 2013, **13**, 4608.
20. K. Das, R. Rawat, B. Satpati, and I. Das, *Appl. Phys. Lett.*, 2013, **103**, 202406.
21. R. B. Yang, C. Y. Tsay, W. F. Liang, and C. K. Lin, *J. Appl. Phys.*, 2010, **107**, 09A523.
22. K. L. Yan, R. H. Fan, Z. C. Shi, M. Chen, L. Qian, Y. L. Wei, K. Sun and J. Li, *J. Mater. Chem. C,* 2014, **2**, 1028.
23. S. Zhang and Q. Cao, *Mater. Sci. Eng. B*, 2012, **177**, 678.
24. M. Faisal, and S. Khasim, *J. Mater Sci: Mater Electron,* 2013, **24**, 2202.
25. S. W. Kim, J. H. Li, J. Kim, and H. W. Lee, *J. Am. Ceram. Soc.*, 2004, **87**, 2213.
26. J. Joo, and C. Y. Lee, *J. Appl. Phys.*, 2000, **88**, 513.

27. Y. K. Vekilov and Y. M. Mukovskii, *Solid State Commun.* 2012, **152**, 1139.
28. A. M. Nicolson, and G. F. Ross, *IEEE Trans. Instrum. Meas*., 1970, **19**, 377.
29. S. H. Park, P. T. Theilmann, M. Asbeck, and P. R. Bandaru, *IEEE Trans. Nanotechnol*., 2010, **9**, 464.
30. X. S. Feng, C. H. Ye, T. Xie, Z. Y. Wang, J. W. Zhao, and L. D. Zhang, *Appl. Phys. Lett*., 2006, **88**, 013101.
31. L. Deng, L. Ding, K. Zhou, S. Huang, Z. Hu, and B. Yang, *J. Magn. Magn. Meter.*, 2011, **323**, 1895.
32. L. Kong, X. Yin, Q. Li, F. Ye, Y. Liu, G. Duo, and X. Yuan, *J. Am. Ceram. Soc.*, 2013, **96**, 221.
33. D. A. Durkee, H. B. Eitouni, E. D. Gomez, M. W. Ellsworth, A. T. Bell, and N. P. Balsara, *Adv. Mater.*, 2005, **17**,2003.
34. Z. Liu, G. Bai, Y. Huang, Y. Ma, F. Du, F. Li, T. Guo, and Y. Chen, *Carbon*, 2007, **45**, 821.
35. R. P. Pawar, R. N. Jadhav, and V. Puri, *Electron. Mater. Lett*., 2012, **8**, 32.
36. S. M. Abbas, R. Chatterjee, A. K. Dixit, A. V. Kumar, and T. C. Goel, *J. Appl. Phys*., 2007, **101**, 074105.
37. Y. L. Cheng, J. M. Dai, X. B. Zhu, D. J. Wu, Z. R. Yang, Y. P. Sun, *Nanoscale Res. Lett*., 2009, **4**, 1153.
38. A. Cao, Z. Liu, S. Chu, M. Wu, Z. Ye, Z. Cai, Y. Chang, S. Wang, Q. Gong, and Y. Liu, *Adv. Mater.*, 2010, **22**, 103.
39. Z. S. Wu, W. Ren, L. Wen, L. Gao, J. Zhao, Z. Chen, G. Zhao, F. Li, and H. M. Cheng, *ACS Nano*, 2010, **4**, 3187.
40. Y. J. Chen, F. Zhang, G. G. Zhao, X. Y. Fang, H. B. Jin, P. Gao, C. L. Zhu, M. S. Cao, and G. Xiao, *J. Phys. Chem. C*, 2010, **114**, 9239.
41. G. Zhou, D. W. Wang, F. Li, L. Zhang, N. Li, Z. S. Wu, L. Wen, G. Q. Lu, and H. M. Cheng, *Chem. Mater*., 2010, **22**, 5306.
42. G. Tong, W. Wu, Q. Hua, Y. Miao, J. Guan, and H. Qian, *J. Alloys Comp*., 2011, **509**, 451.
43. G. Tong, J. Ma, W. Wu, Q. Hua, R. Qiao, and H. Qian, *J. Mater. Res.*, 2011, **26**, 682.
44. J. Huo, L. Wang, H. Yu, *J. Mater. Sci*., 2009, **44**, 3917.
45. A. Ohlan, K. Singh, A. Chandra, V. N. Singh, and S. K. Dhawan, J. Appl. Phys., 2009, **106**, 044305.
46. S. W. Phang, T. Hino, M. H. Abdullah, and N. Kuramoto, *Mater. Chem. Phys*., 2007, **104**, 327.
47. X. F. Zhang, X. L. Dong, H. Huang, Y. Y. Liu, W. N. Wang, X. G. Zhu, B. Lv, J. P. Lei, and C. G. Lee, *Appl. Phys. Lett*., 2006, **89**, 053115.
48. C. L. Zhu, M. L. Zhang, Y. L. Qiao, G. Xiao, F. Zhang, and Y. J. Chen, *J. Phys. Chem. C,* 2010, **114**, 16229.
49. N. C. Das, D. Khastgir, T. K. Chaki, and A. Chakraborty, *Composites Part A: Appl. Sci. Manufact*., 2000, **31**, 1069.
50. M. H. Al-Saleh, and U. Sundararaj, *J. Phys. D: Appl. Phys*., 2013, **46**, 035304.
51. P. Saini, V. Choudhary, B. P. Singh, R. B. Mathur, and S. K. Dhawan, Synthetic Metals, 2011, **161**, 1522.
52. W. H. Otto, "Electromagnetic compatibility engineering," New Jersey, John Wiley & Sons. (2009)
53. D. Micheli, R. Pastore, C. Apollo, M. Marchetti, G. Gradoni, V. M. Primiani, and F. Moglie, *IEEE Trans. Microw. Theory Tech.*, 2011, **59**, 2633.
54. D. Micheli, C. Apollo, R. Pastore, D. Barbera, R. B. Morles, M. Marchetti, V. M. Primiani, and F. Moglie, *IEEE Trans. Electromagn. Compat.*, 2012, **54**, 60.
55. D. Micheli, R. Pastore, A. Vricella, R. B. Morles, M. Marchetti, A. Delfini, F. Moglie, V. M. Primiani, *Mater. Sci. Engg. B*, 2014, **188**, 119.
56. S. Lucyszyn, and Y. Zhou, *Prog. Electromagn. Res*., 2010, **103** 17.
57. A. P. Singh, P. Garg, F. Alam, K. Singh, R. B. Mathur, R. P. Tandon, A. Chandra, and S. K. Dhawan, *Carbon*, 2012, **50**, 3868.

EMI shielding effectiveness up to 19 dB observed in LSMO nanomaterials